Environment Canada

Environnement Canada

National Water Research Institute

Institut National de Recherche sur les Eaux

This manuscript has been presented to the Scripps Institution of Oceanography Advanced Study Program, December 1983, on the topic of "Interactions of the Atmosphere and the Upper Ocean" and will be published in a series by Springer-Verlag.

This copy is to provide information prior to publication.

FREQUENCY AND WAVENUMBER SPECTRA OF WIND-GENERATED WAVES

by

Mark A. Donelan

Shore Processes Section
Hydraulics Division
National Water Research Institute
Canada Centre for Inland Waters
Burlington, Ontario, Canada L7R 4A6

October 1984

ABSTRACT

From observations of wind and of water surface elevation at 14 wave staffs in an array in Lake Ontario and in a large laboratory tank, the directional spectrum of wind-generated waves on deep water is determined. Systematic investigations reveal the following: (a) the frequency spectrum in the rear face is proportional to the minus 4 power of the frequency ω with the equilibrium range parameter and the peak enhancement factor clearly dependent on the ratio of wind speed to peak wave speed; (b) the angular spreading θ of the wave energy is of the form $\text{sech}^2\ \beta\theta$, where β is a function of frequency relative to the peak; (c) depending on the gradient of the fetch, the direction of the wave at the spectral peak may differ from the mean wind direction by up to 50°, but this observed difference is predictable by a similarity analysis; (d) under conditions of strong wind forcing, significant effects on the phase velocity due to amplitude dispersion and the presence of bound harmonics are clearly observed which are in accordance with Stokes' theory, whereas (e) the waves under natural wind conditions show amplitude dispersion, but bound harmonics are too weak to be detected among the background of free waves.

RESUME

Le spectre des directions des vagues engendrées par le vent en eau profonde est déterminée à partir d'observations du vent et du niveau de l'eau faites à l'aide d'un réseau de 14 tiges rigides placées dans le lac Ontario et dans un grand réservoir en laboratoire. Des études systématiques ont montré que: a) le spectre des fréquences à l'arrière du réseau est proportionnel à l'inverse de la puissance 4 de la fréquence ω, le paramètre d'équilibre de la gamme et le facteur de renforcement du maximum dépendant clairement du rapport vitesse du vent/vitesse maximale de la vague; b) l'étalement angulaire θ de l'énergie des vagues est de la forme $\text{sech}^2 \beta\theta$, où β est une fonction de la fréquence par rapport au maximum; c) selon le gradient de la course du vent, la direction de la vague au maximum du spectre peut s'écarter de 50° ou plus de la direction moyenne du vent, mais cette différence observée peut être prévue par une analyse des similitudes; d) dans les d'oscillations forcées par un vent puissant, des effets significatifs sur la vitesse des phases due à la dispersion de l'amplitude et à la présence d'harmoniques en rapport avec l'onde principale, en accord avec la théorie de Stokes, apparaissent clairement; alors que e) les vagues, dans des conditions de vent normal, présentent une dispersion d'amplitude mais leurs harmoniques sont trop faibles pour être décelés, compte tenu de la présence d'oscillations libres.

MANAGEMENT PERSPECTIVE

Prediction of wave heights in lakes and limited fetch seas - such as the Beaufort Sea - generally assumes that wind and wave direction are the same. This paper shows that this is not true and also shows how to estimate the true wave direction.

Wave direction is required for many studies, shore erosion, transport of nearshore pollutants, safety of structures and navigation. This paper provides a great improvement in analysis.

T. Milne Dick
Chief
Hydraulics Division

PERSPECTIVE DE GESTION

Le prévision des hauteurs des vagues dans les lacs et les mers où la course du vent est limitée, par exemple la mer de Beaufort, présuppose généralement que les vagues et le vent vont dans la même direction. Le présent article démontre le contraire et indique comment évaluer la direction réelle des vagues.

Le présent article améliore grandement l'analyse de la direction des vagues, qui est nécessaire pour de nombreuses études et de nombreux problèmes comme l'érosion des rives, le transport côtier des polluants, ainsi que la sécurité des structures et de la navigation.

T. Milne Dick
Chef
Division de l'hydraulique

FREQUENCY AND WAVENUMBER SPECTRA OF WIND-GENERATED WAVES

by Mark A. Donelan

1.0 INTRODUCTION

This paper is based on collaborative work with J. Hamilton and W.H. Hui. A complete description of our observations of various aspects of the directional spectra will shortly be published (Donelan et al. 1984). In the following pages I shall summarize some of the more significant findings of this much longer work.

These observations of wind-generated waves in Lake Ontario were made to examine the fetch-dependence of the frequency and wavenumber spectra. We were particularly interested in determining the disperion relation, the directional spreading function and a concise parametric description of the frequency spectrum, and to see how these were affected by fetch or wave age, i.e., the ratio of phase speed of the waves at the spectral peak to the wind speed. At the conclusion of the field observations we took our apparatus (somewhat scaled down) inside to a large laboratory wind-wave tank to extend our range of conditions to very low wave age and correspondingly high wave steepness. Of particular interest here was the effect of steepness on the dispersion relation.

The Stokes' (1847) expansion appropriate to a surface gravity wave of permanent form on deep water yields surface elevation, ζ, which to fourth order in wave slope ak, is (Hui and Tenti, 1982):

$$\begin{aligned}\zeta k = {} & ak\cos(kx - \omega t) + \{1/2(ak)^2 + 17/24(ak)^4\}\cos 2 \cdot \\ & (kx - \omega t) + 3/8(ak)^3 \cos 3(kx - \omega t) + 1/3(ak)^4 \cdot \\ & \cos 4(kx - \omega t) \end{aligned} \quad (1)$$

National Water Research Institute, Canada Centre for Inland Waters, P.O. Box 5050, Burlington, Ontario, Canada

where k is the radian wave number, ω the radian wave frequency and x the propagation direction. The time history of surface elevation at a point corresponding to such a Stokes' wave is given in Figure 1 accompanied by actual observations of wind-generated waves in a large laboratory tank. The characteristic sharp crests and flattened troughs are evident and imply the existence of bound harmonics, i.e., disturbances having wavenumbers which are multiples of the fundamental wavenumber and which travel at the same phase speed ($c = \omega/k$) as the fundamental as described by (1). The dispersion relation corresponding to the Stokes' wave (1) is:

$$\omega^2 = gk \{1 + (ak)^2 + 5/4(ak)^4\} \qquad (2)$$

The maximum value of the wave steepness is about .44 so that the steepest waves will travel about 11% faster than the equivalent infinitesimal wave ($ak \ll 1$). The whole system - fundamental and bound harmonics - travels at the steepness-enhanced speed of the fundamental. Such a system of waves is "non-dispersive". On the other hand, a wave field comprised of a collection of free waves will be dispersive with speed inversely related to frequency or to wavenumber. As we shall see later, the laboratory experiments were very useful in illustrating the relative importance of bound and free waves on the rear face of the spectrum.

The second aspect of the directional spectra - the directional spreading - is based entirely on the field observations since the laboratory flows, being constrained by the tank walls, are not suitable models of the three-dimensional aspects of the natural processes.

Finally we examine the fetch or wave age dependence of the parameters of the frequency spectrum and find that in the energy containing (99%) part of the spectrum the rear face is in close agreement with an ω^{-4} power law. A spectral description based on this

shows considerable sharpening of the peak at short fetch (young waves) and asymptotic agreement with observations of fully developed spectra.

2.0 OBSERVATIONS AND EXPERIMENTS

The map (Figure 2) shows the location of the observation platform in the western end of Lake Ontario. The platform (a bottom mounted tower - Figure 3) stands in 12 metres of water and commands fetches of 1.1 km to 300 km. Meteorological instruments, on a tower in the centre of the platform, measure means and variances of wind velocity components, temperature and humidity, while an array of capacitance wave staffs (Figure 4) provides 14 coincident time series of surface elevation for later decomposition into wavenumber-frequency spectra.

After the field observations a laboratory experiment was conducted using a 1/28 scaled version of the array in the large wind-wave tank of the Canada Centre for Inland Waters (Figure 5).

3.0 DIRECTIONAL SPECTRA AND DISPERSION RELATIONS

Six spectra of varying wave age are illustrated on logarithmic axes in Figure 6. The parameter U_c/c_p is approximately the inverse of the wave age except that the component of the wind velocity parallel to the propagation direction of the waves at the spectral peak is used instead of the wind speed itself. $U_c = U_{10} \cos \theta$, where θ is the angle between wave direction of the spectral peak and the wind direction. c_p is the phase speed of the waves at the spectral peak frequency, ω_p. With increasing U_c/c_p the frequency spectra become noticeably narrower with relatively more energy concentrated near the peak. The youngest (laboratory waves) show secondary peaks at $n\omega_p$ which are, as we will demonstrate, associated with bound harmonics.

The wavenumber-frequency spectrum $X(\underset{\sim}{k},\omega)$ is the Fourier transform of the space-time covariance of surface displacement $\rho(\underset{\sim}{r},t)$:

$$X(\underset{\sim}{k},\omega) = (2\pi)^{-3} \iiint \rho(\underset{\sim}{r}, t) \exp[-i(\underset{\sim}{k}\cdot\underset{\sim}{r} - \omega t)]\, d\underset{\sim}{r}\, dt \quad (3)$$

where $\underset{\sim}{r}$ is the horizontal separation vector. Illustrative examples of $X(\underset{\sim}{k}, \omega_j)$ are given for six frequencies ω_j in Figure 7. These are relatively mature field waves ($U_c/c_p = 1.5$). The solid circles are the deep water dispersion relation for infinitesimal waves ($k = \omega^2/g$) for the limits of the frequency bands ω_j. The broken circles correspond to the (energy) centroidal frequencies of the bands. The frequency spectrum is shown in the top left corner of the figure.

These contour diagrams illustrate the strong directionality of the waves near the peak of the spectrum and a appreciable broadening with increasing frequency away from the peak. A clockwise rotation of the wavenumber spectra is also apparent and, as will be shown in Section 6, this is typical of the alignment of the short (high frequency) waves with the wind direction, whereas the direction of the longer waves near the peak is related to the upwind fetch distribution.

Strict obedience to the linear (infinitesimal slope) dispersion relation requires that the contours of $X(\underset{\sim}{k}, \omega_j)$ fall within the solid circles. It can be seen that while most of the energy lies between the circles (Figure 7) some falls inside the smaller circle and this tendency becomes more pronounced with increasing fequency. Thus the average wavenumber is smaller than the (linear) theoretical one and the phase speed correspondingly higher. The increase in phase speed is only a few percent and is believed to be the effect of amplitude dispersion described by (2). By contrast Figure 8 illustrates the pattern of the high frequency wavenumber spectra when bound harmonics are larger than the corresponding free waves at that frequency. In panels (e) and (f) the energy is concentrated inside the linear dispersion circles. The wavenumbers of harmonics bound to the peak k_b are considerably smaller than the corresponding free wavenumbers, k_f:

$$\frac{k_b}{k_f} = \frac{1}{n} \quad ; \quad n = 2,3 \ldots \tag{4}$$

where n is the harmonic number.

Apparently the energy in panels (e) and (f) of Figure 8 is closely associated with bound harmonics. Any free wave energy present is sufficiently low that it is missed by the lowest contour, i.e., 12.5% of the peak value in any panel. The presence of free and bound waves in the same frequency band is seen in panel (d), where the free energy is shifted towards lower wavenumbers by about 10% corresponding to strong amplitude dispersion. Nearer the peak (panels (a), (b) and (c)) free waves only are evident with varying amounts of amplitude dispersion.

The pronounced bound harmonics of Figure 8 are associated with very steep waves near the spectral peak and this is reflected in the strongly peaked frequency spectrum shown in the figure, which may be compared with the much broader spectrum of Figure 7.

An average wavenumber may be computed from the wavenumber spectra by integrating over wavenumber magnitude and angle θ:

$$\bar{k}(\omega_j) = \frac{\iint k \, X(\underset{\sim}{k},\omega_j) \, dk \, d\theta}{\iint X(\underset{\sim}{k},\omega_j) \, dk \, d\theta} \tag{5}$$

where $\underset{\sim}{k} = k(\cos\theta, \sin\theta)$.

From this an 'average phase speed' ($\bar{c}_j = \omega_j / \bar{k}$) may be determined and this has been graphed in Figure 9. The mature waves ($U_c/c_p = 1.0$) are in agreement with the linear dispersion relation near the peak frequency but at higher frequencies ($\omega/\omega_p > 1.5$) there is evidence of amplitude dispersion. The younger waves ($U_c/c_p > 3$) exhibit amplitude dispersion at and above the peak frequency. The phase speeds of the youngest laboratory waves ($U_c/c_p > 11$) deviate markedly from the linear theory with the

waves at twice the peak frequency travelling at about the speed of the waves at the peak. This almost non-dispersive result is a consequence of lumping free and bound waves together in the determination of (5). The implication of Figure 9 is that for large U_c/c_p the wave field consists of steep waves in a narrow band around the peak frequency with an attendant system of bound harmonics. If the bound harmonics are isolated (Donelan et al. 1984) and the phase speeds of the remaining free waves calculated, the resulting dispersion curves (Figure 10) demonstrate that free waves are always present with varying amounts of amplitude dispersion. In fact Donelan et al. (1984) have shown that for $U/c_p > 9$ the energy in the bound harmonics exceeds that in the free waves at twice the peak frequency and above. Such high values of U/c_p occur only at very short fetch or fleetingly following a sudden change in the wind. Thus for most descriptions of natural waves (2) yields the dispersion relation adquately; where the steepness, ak is a function of U/c_p and ω/ω_p (Donelan et al. 1984).

4.0 DIRECTIONAL SPREADING

Directional spectra are more often used in polar (frequency-direction, $F(\omega,\theta)$) form than in wavenumber-frequency form $X(\underset{\sim}{k},\omega)$.

$$F(\omega_j,\theta) = \int_0^\infty X(\underset{\sim}{k}, \omega_j)\, k\,dk \qquad (6)$$

Polar spectra from six frequency bands, ω_j, of a single case are illustrated in Figure 11. Both the directional broadening of the spectra and the shift towards alignment with the wind direction are apparent in the figure. The frequency spectra were almost always single peaked and eighty-four such spectra were obtained and analyzed in the form of Figure 11. The polar spectra were also uni-modal and Donelan et al. (1984) found that the directional spreading was best described by:

$$F(\omega,\theta) = \frac{1}{2}\,\phi(\omega)\,\beta\,\mathrm{sech}^2\,\beta\,\{\theta - \bar{\theta}(\omega)\} \qquad (7)$$

where $\phi(\omega)$ is the frequency spectrum, $\bar{\theta}$ is the mean wave direction and β, the spreading parameter, is given by:

$$\beta = \begin{cases} 2.61\,(\frac{\omega}{\omega_p})^{+1.3} & ; \quad 0.56 < \frac{\omega}{\omega_p} < 0.95 \\ 2.28\,(\frac{\omega}{\omega_p})^{-1.3} & ; \quad 0.95 < \frac{\omega}{\omega_p} < 1.6 \\ 1.24 & ; \quad \text{otherwise} \end{cases} \qquad (8)$$

Thus the spreading is least just below the peak frequency ($\omega/\omega_p = 0.95$) and increases on the forward and rear faces. Under steady wind conditions the mean wave direction $\bar{\theta}(\omega)$ depends on the upwind fetch distribution and the frequency ω. High frequency waves are generally closely aligned with the wind (Figure 11). A method for predicting the offwind angle of the most energetic waves is given in Section 6.

5.0 FREQUENCY SPECTRA

The frequency spectra of all cases (84 field and 7 laboratory) have been grouped by the parameter U_c/c_p and graphed in Figure 12. The smooth variation in width and general similarity of the spectra support the idea that wind-generated spectra may be described using a similarity framework such as proposed by Kitaigorodskii (1962). The most apparent characteristic of the spectra is the systematic narrowing with increase in U_c/c_p. This is largely due to the enhancement of the peak of the spectrum (Figure 13). The rear face or equilibrium range of the spectra was found to depend on ω^{-4} rather than ω^{-5} as originally proposed by Phillips

(1958). More recently other researchers (e.g., Toba, 1973; Forristall, 1981; Kahma, 1981) have observed ω^{-4} equilibrium ranges in the energy containing part of the spectrum. At higher frequencies the effects of Doppler shifting by currents and wave orbital velocities reduce the likelihood of an universal equilibrium range in frequency spectra. However, in the range of frequencies ($1.5\ \omega_p < \omega < 3\ \omega_p$) illustrated in Figure 13 these effects are small and the ω^{-4} dependence described the rear face well. Normalization by the average spectral level on the rear face reveals the pronounced enhancement of the peak at high U_c/c_p. Hasselmann et al. (1973) modified the form of the fully developed spectrum given by Pierson and Moskowitz (1964) to include the enhancement of the peak. We have modified their compact spectral description to include the observed ω^{-4} rear face (Donelan et al. 1984) and found that the spectral parameters were well correlated with the inverse wave age, U_c/c_p. The frequency spectrum $\phi(\omega)$ is described thus:

$$\phi(\omega) = \alpha\, g^2\, \omega^{-5} \left(\frac{\omega}{\omega_p}\right) \exp\left\{-\left(\frac{\omega_p}{\omega}\right)^4\right\} \cdot \gamma^{\exp\left\{-\frac{(\omega-\omega_p)^2}{2\sigma^2\omega_p^2}\right\}} \qquad (9)$$

where α, the equilibriumn range parameter, γ, the peak enhancement factor and σ, the spectral width parameter are given by:

$$\alpha = 0.006 \left(\frac{U_c}{c_p}\right)^{0.55} \quad ; \quad 0.83 < \frac{U_c}{c_p} < 5 \qquad (10)$$

$$\gamma = \begin{cases} 1.7 & ; \quad 0.83 < \dfrac{U_c}{c_p} < 1 \\ 1.7 + 6.0 \log_{10}\left(\dfrac{U_c}{c_p}\right) & ; \quad 1 \leq \dfrac{U_c}{c_p} < 5 \end{cases} \qquad (11)$$

$$\sigma = 0.08\,[1 + 4/(\frac{U_c}{c_p})^3] \quad ; \quad 0.83 < \frac{U_c}{c_p} < 5 \qquad (12)$$

In Figure 14 we compare the JONSWAP (Hasselmann et al. 1973) and Pierson-Moskowitz (1964) spectra with the spectra represented by (9). Two values of U/c_p (4 and 0.83) are shown corresponding to non-dimensional fetches (xg/U_c^2) of 10^2 (fetch-limited) and 10^5 (fully-developed). The values of wind speed and fetch appropriate to these spectra (ω_p = 2.5) are respectively 15.6 m/s and 2.5 km (fetch-limited) and 3.2 m/s and 104 km (fully-developed). The Pierson-Moskowitz spectrum applies only to full development, and it is encouraging that the spectrum of (9), derived largely from fetch-limited data, is in good agreement with the Pierson-Moskowitz. At the other end of the scale of strongly fetch-limited spectra, the JONSWAP spectrum is in reasonable agreement with (9). However, the JONSWAP spectrum, extrapolated to full development, retains its enhanced peak and is therefore unable to relax to the broader peaked fully-developed spectrum. The differences between the JONSWAP spectrum and (9) hinge on the choice of the power law for the rear face of the spectrum.

6.0 NON-DIMENSIONAL FETCH AND WAVE DIRECTION

Figure 15 shows the dependence of non-dimensional fetch $\tilde{x}$ on U_c/c_p over five orders of magnitude in $\tilde{x}$. Fetch $x(\theta)$ is the fetch in the direction of propagation of the waves at the spectral peak. Field and laboratory data are nearly contiguous, but a power law (solid line) fitted to the field data clearly does not represent the laboratory results. The laboratory data fall on a line (dotted) which is displaced upward and to the right of the power law representing the field data. Phillips (1977) has remarked that the laboratory and field data summarized by Hasselmann et al. (1973) do not necessarily

conform to the same similarity law and fitted a power law (shown dashed) to their field data only.

For our field data the empirical relationship linking non-dimensional fetch and U_c/c_p is:

$$\frac{U \cos \theta}{c_p} = 11.6 \tilde{x}^{-0.23} \qquad (13)$$

Both in the execution of steady-state fetch-limited experiments and in the application of fetch-limited formulae in hindcasting, it is common practice to assume that the mean wave propagation direction agrees with the wind direction. That this cannot be true in general is evident from the fact that waves are not strictly locally generated, but instead are the net result of their development along the entire upwind fetch. If, therefore, the gradient of fetch about the wind direction is large one might reasonably expect the wave direction to be biased towards long fetch, where the reduced generating force of the lower wind component (U cos θ) is more than balanced by the longer fetch over which it acts. In Figure 16 the observed mean direction of the waves near the peak of the spectrum is plotted against average wind direction. The straight line (dashed) is the line of perfect agreement with the wind direction. When the fetch gradient is small - wind directly offshore (-120°) or along the long axis of the lake (75°) - the wave and wind directions agree. Otherwise, the discrepancies can be as much as 50°. Certainly such differences call into question the validity of hindcasting techniques which disregard them.

Initial attempts to use Kitaigorodskii's scaling law for non-dimensional frequency with fetch in the wind direction produced a much poorer correlation than that of Figure 15. This supports the view that, unless the wind is blowing directly offshore from a straight shoreline, more appropriate parameters for similarity scaling are the fetch and wind component in the wave direction rather than the

wind direction. The similarity relation of (13) may be written in terms of the peak period T_p:

$$T_p = 0.54\, g^{-0.77}\, U^{0.54} (\cos\theta)^{0.54}\, x^{0.23} \qquad (14)$$

where x is the fetch in the wave propagation direction.

Since the energy density at the peak of the spectrum is roughly proportional to T_p^5 (Phillips 1977, Figure 4.8), it is clear that the direction (θ) which yields the largest value of T_p from (14) will be the direction of approach of the waves at the peak of the spectrum.

For any wind speed U such that the waves are fetch-limited, the righthand side of (14) ($\cos\theta \cdot x^{0.426}$) may be maximized to yield the offwind angle θ of approach of the peak of the spectrum. Running averages of the geometric fetch at one degree increments over various windows from ±0 to ±30° were computed and used to deduce the peak wave approach direction. The sensitivity to width of averaging window was not large as demonstrated in the inset to Figure 16 for window widths of 0 and 60 degrees. The best agreement (solid line in Figure 16) with the observed wave approach direction was achieved with window width of 30°, i.e., ±15 degrees on either side of θ.

7.0 REFERENCES

Donelan, M.A., J. Hamilton, and W.H. Hui. 1985. Directional Spectra of Wind-Generated Waves. Phil. Trans. Roy. Soc. (in press).

Forristall, G.Z. 1981. Measurements of a Saturated Range in Ocean Wave Spectra. J. Geophys. Res., 86, C9, pp. 8075-8084.

Hasselmann, K., T.P. Barnett, E. Bouws, H. Carlson, D.E. Cartwright, K. Enke, J.A. Ewing, H. Gienapp, D.E. Hasselmann, P. Kruseman, A. Meerburg, P. Müeller, D.J. Olbers, K. Richter, W. Sell, and H. Walden. 1973. Measurements of Wind-Wave Growth and Swell Decay During the Joint North Sea Wave Project (JONSWAP). Dtsch. Hydrogr. Z., A8 (Suppl.), No. 12.

Hui, W.H. and G. Tenti. 1982. A New Approach to Steady Flows with Free Surfaces. J. Appl. Math. and Physics (ZAMP), 33, pp. 569-589.

Kahma, K.K. 1981. A Study of the Growth of the Wave Spectrum with Fetch. J. Phys. Oceanogr., 11, pp. 1503-1515.

Kitaigorodskii, S.A. 1962. Applications of the Theory of Similarity to the Analysis of Wind-Generated Wave Motion as a Stochastic Process. Bull. Acad. Sci., USSR Geophys. Ser. 1, pp. 105-117.

Phillips. O.M. 1958. The Equilibrium Range in the Spectrum of Wind-Generated Waves. J. Fluid Mech., 4, pp. 426-434.

Phillips. O.M. 1977. The Dynamics of the Upper Ocean. 2nd Edition, Cambridge University Press, Cambridge, 336 pp.

Pierson, W.J. and L. Moskowitz. 1964. A Proposed Spectral Form for Fully Developed Wind Seas Based on the Similarity Theory of S.A. Kitaigorodskii. J. Geophys, Res., 69, pp. 5181-5190.

Stokes, G.G. 1847. On the Theory of Oscillatory Waves. Trans. Camb. Phil. Soc., 8, pp. 441-455.

Toba, Y. 1973. Local Balance in Air-Sea Boundary Processes III. On the Specrum of Wind Waves. J. Oceanogr. Soc. Japan, 29, pp. 209-220.

FIGURE CAPTIONS

1. Stokes' wave (a) and a record of the time history of surface elevation in a wind-wave tank (b) at fetch of 50 m and wind speed of 11 m/s.

2. Map showing the location of the research tower in Lake Ontario and the shore-normal profile in the vicinity of the tower.

3. Photograph of the research tower. The wave staffs can be seen suspended from the tower itself and from its extensions in three directions. Meteorological instruments are mounted on a mast at the centre and the measuring and communications devices are housed in the box at the foot of the mast.

4. Location of wave staffs in the array.

5. Plan of the wind-wave flume. The location of the directional wave array is indicated by an X labelled "D.S.". The lower part of the figure shows an enlargement of the directional array and its orientation in the flume.

6. Log-log spectra for three runs of field waves (bottom) and three runs of laboratory waves. With increasing U_c/c_p the spectra become narrower and acquire secondary peaks at $n\omega_p$. The 90% confidence limits are indicated by a vertical bar.

7. Wavenumber spectra $X(\underset{\sim}{k},\omega)$, (3) for a relatively mature spectrum of field waves. The percent energy in each frequency band is indicated. Note that the energy falls within the dispersion circles near the peak, but moves inwards at higher frequencies. θ is the angle between wind and propagation direction of the waves at the peak of the spectrum.

8. Wavenumber spectra for very young laboratory waves. Evidence for bound harmonics can be seen in (d), (e) and (f).

9. Normalized average phase speed versus ω/ω_p for five spectra. The two at the bottom of the figure are from field data, the others from laboratory data. As U_c/c_p increases the effects of bound harmonics are apparent. The normalizer c_p is the theoretical linear phase speed of the peak waves $c_p = g/\omega_p$.

10. Normalized phase speed of free waves for the same five spectra as in Figure 9. The effects of amplitude dispersion with increasing U_c/c_p are apparent.

11. Directional (or polar) spectra $F(\omega,\theta)$, (6) corresponding to the wavenumber spectra of Figure 7. The dashed line is a measure of the error in the estimation of F; the vertical scale is arbitrary.

12. Normalized frequency spectra grouped into classes by U_c/c_p. The vertical bars at the top of the figure are an estimate of the 90% confidence limits based on the standard error of the mean.

13. Frequency spectra x ω^4 normalized by the rear face $[\omega^4\phi(\omega)]_{R.F.}$ which is the average of $\omega^4\phi(\omega)$ in the region $1.5\ \omega_p < \omega < 3\omega_p$. The lines corresponding to ω^{-5} and ω^{-3} are also shown (—— – ——). The effect of a 10 cm/s ambient current with or against the waves is also shown (-----) as is the effect of wind drift in a 10 m/s wind (—— ——). The spectra are grouped in classes of U_c/c_p.

14. Comparison of spectra with $\omega_p = 2.5$ for two values of U/c_p or, equivalently, of non-dimensional fetch.

15. Non-dimensional fetch versus U_c/c_p. (——) fit to the field data; (-----) fit to the laboratory data; (— — —) from Phillips (1977).

16. Mean direction of waves at the spectral peak versus mean wind direction (approach bearing in both cases). The broken line is the line of perfect agreement; the solid line has been deduced from similarity considerations (14) using fetch averaged over 30° (±15°) about the wave approach direction. The inset demonstrates the relative insensitivity to choice of averaging over 60° (solid) or not at all (broken).

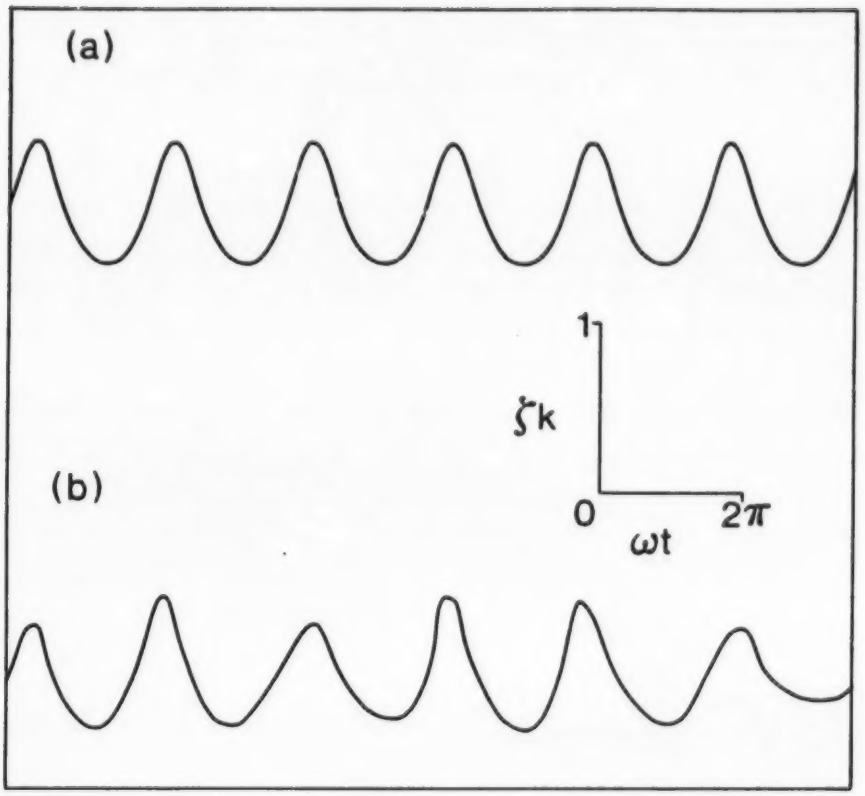
(a)
1
ζk
(b)
0
2π
ωt

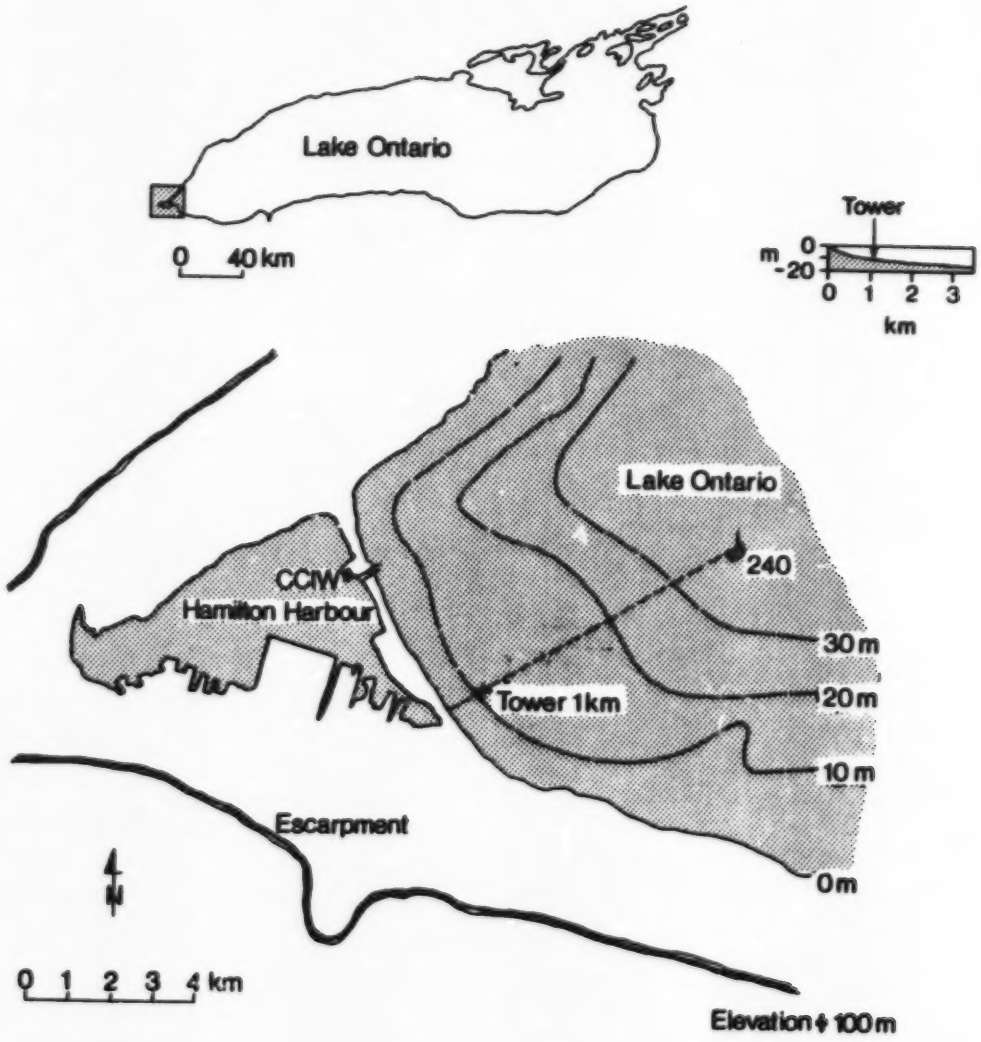
Lake Ontario
0 40 km
Tower
m 0
-20
0 1 2 3
km
Lake Ontario
CCIW
Hamilton Harbour
240
30 m
Tower 1km
20 m
10 m
Escarpment
0 m
N
0 1 2 3 4 km
Elevation ↑ 100 m

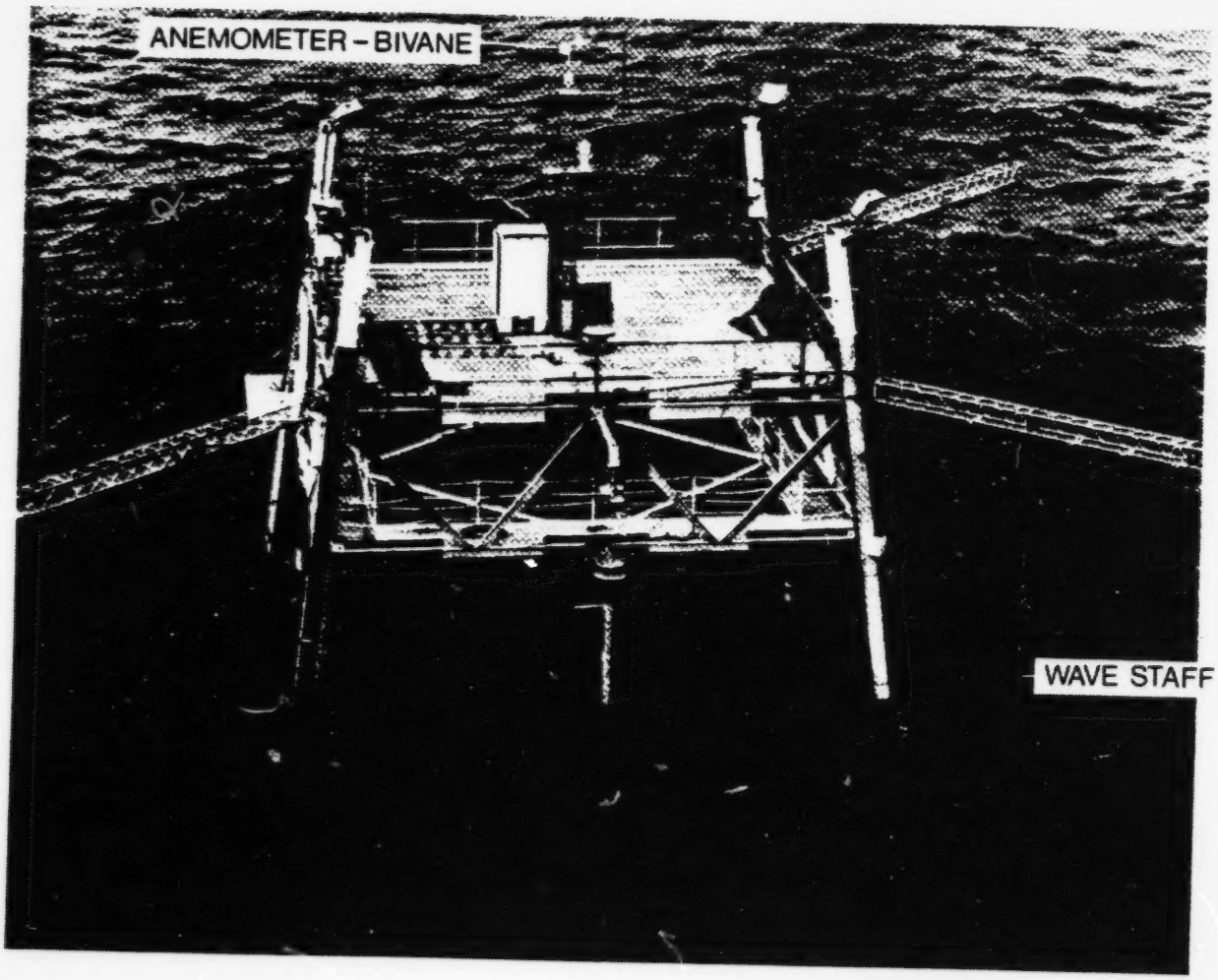
ANEMOMETER – BIVANE
WAVE STAFF

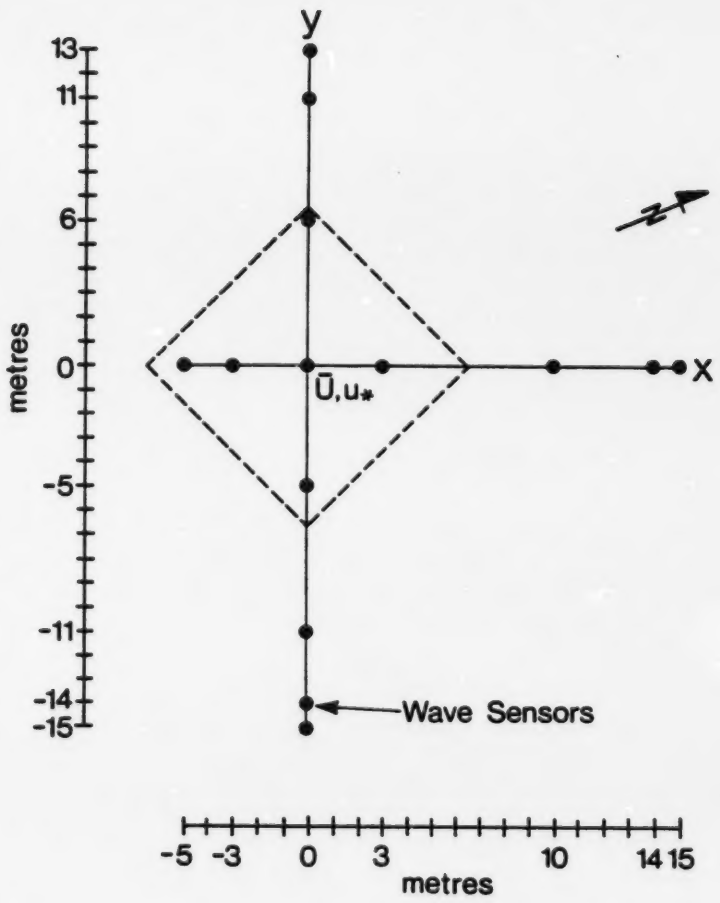
y
13
11
6
0
-5
-11
-14
-15
metres
x
$\bar{U}, u_*$
Wave Sensors
-5 -3 0 3 10 14 15
metres

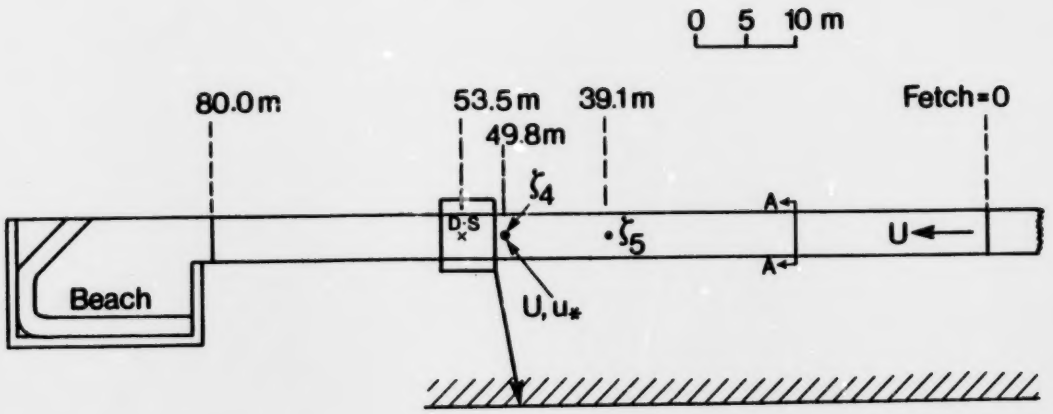
0 5 10 m
80.0 m
53.5 m
49.8 m
39.1 m
Fetch=0
ζ_4
ζ_5
D.S
A
A
U
Beach
U, u_*

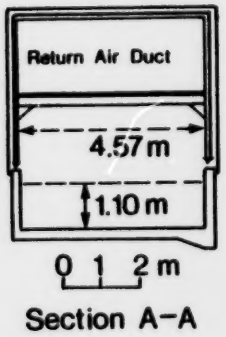
Return Air Duct
4.57 m
1.10 m
0 1 2 m

Section A–A

U

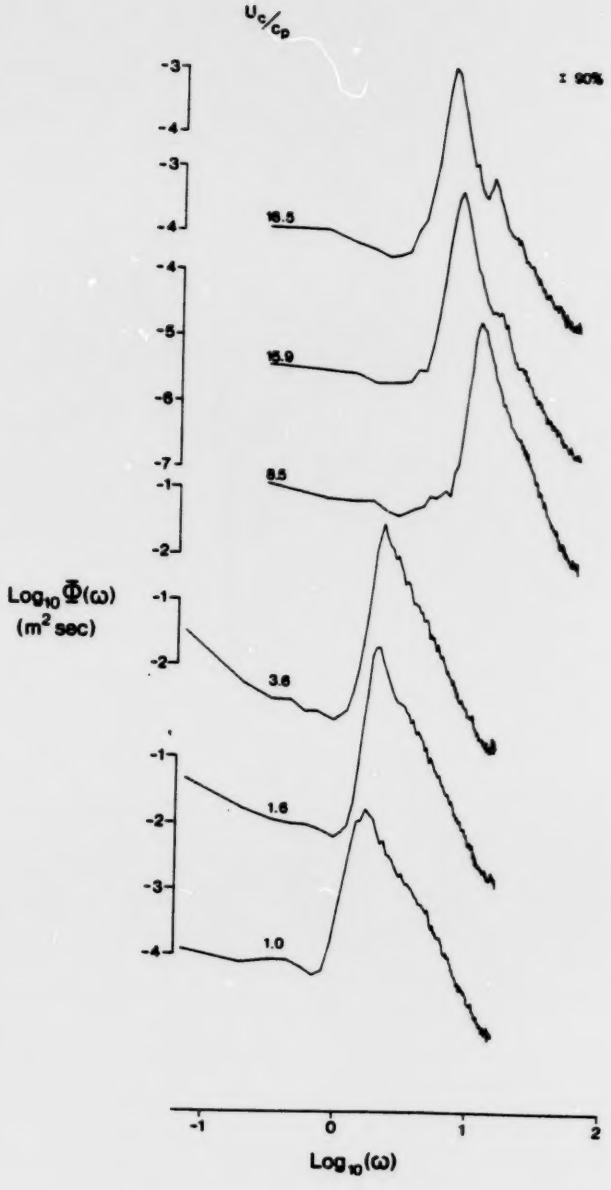
U_c/c_p
± 90%
16.5
15.9
8.5
3.8
1.6
1.0
$\text{Log}_{10}\Phi(\omega)$
(m^2 sec)
$\text{Log}_{10}(\omega)$

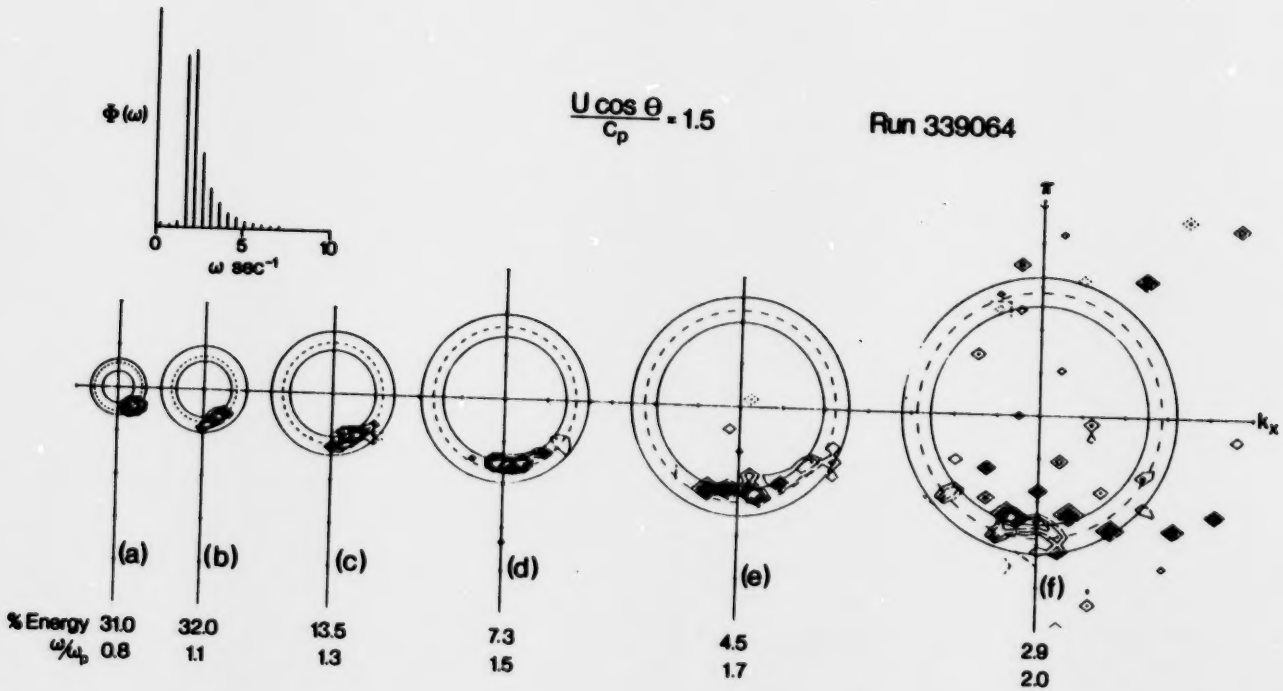
Φ(ω)
0
5
10
ω sec⁻¹
U cos θ / c_p = 1.5
Run 339064
k_x
(a)
(b)
(c)
(d)
(e)
(f)
% Energy 31.0 32.0 13.5 7.3 4.5 2.9
ω/ω_p 0.8 1.1 1.3 1.5 1.7 2.0

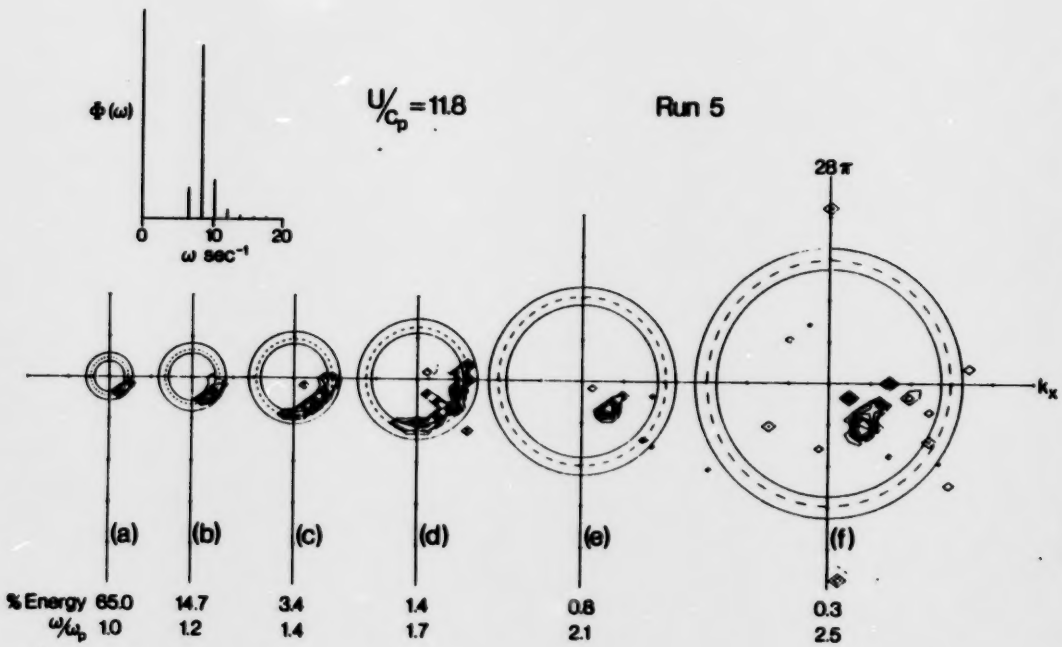
Φ(ω)
0
10
20
ω sec⁻¹
U/Cp = 11.8
Run 5
2.8π
kx
(a)
(b)
(c)
(d)
(e)
(f)
% Energy 65.0 14.7 3.4 1.4 0.8 0.3
ω/ωp 1.0 1.2 1.4 1.7 2.1 2.5

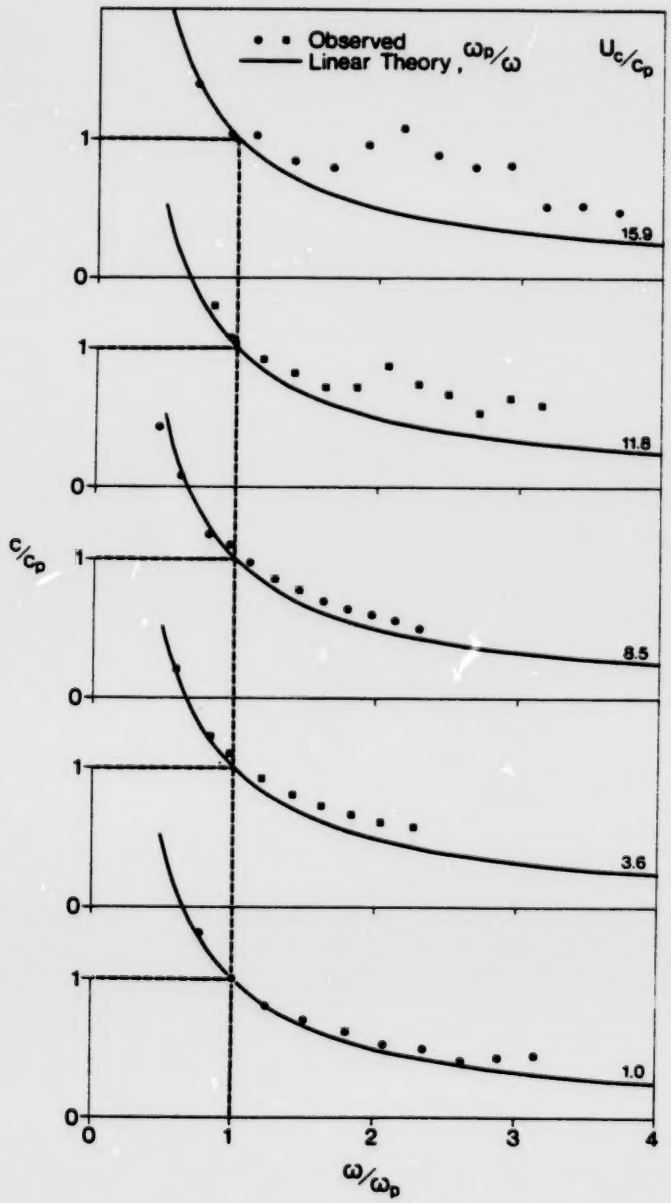
Observed
Linear Theory, ω_p/ω
U_c/c_p
15.9
11.8
8.5
3.6
1.0
c/c_p
0
1
2
3
4
ω/ω_p

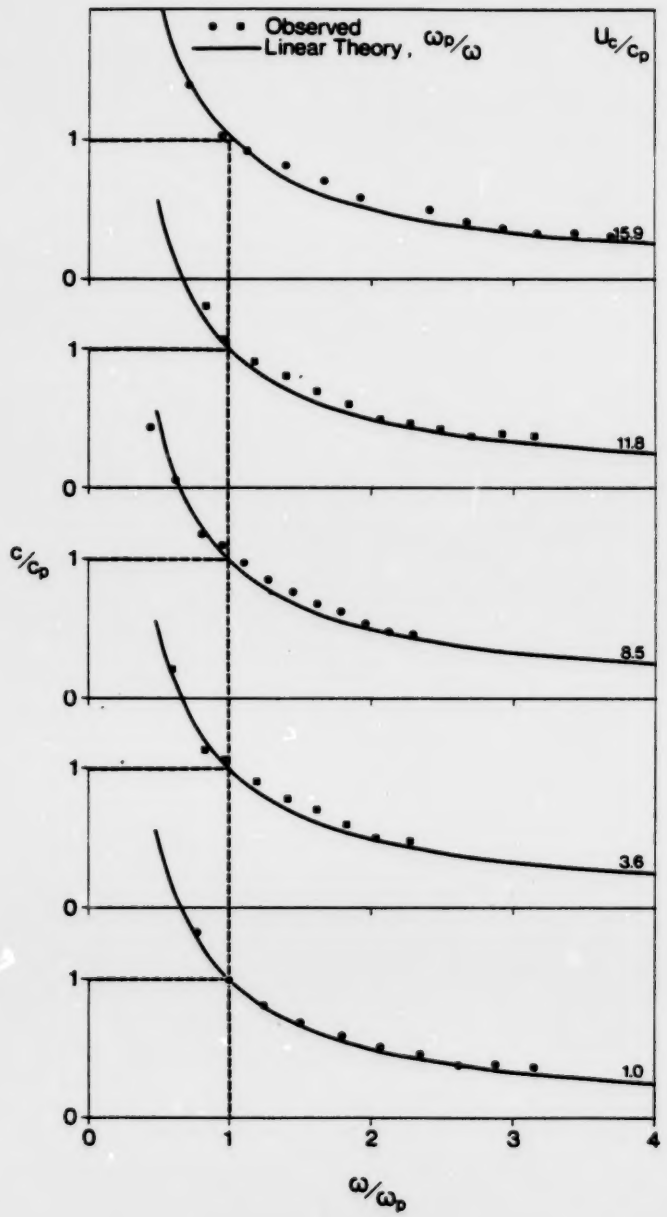
Observed
Linear Theory, ω_p/ω
U_c/c_p
15.9
11.8
8.5
3.6
1.0
c/c_p
ω/ω_p
0
1
2
3
4

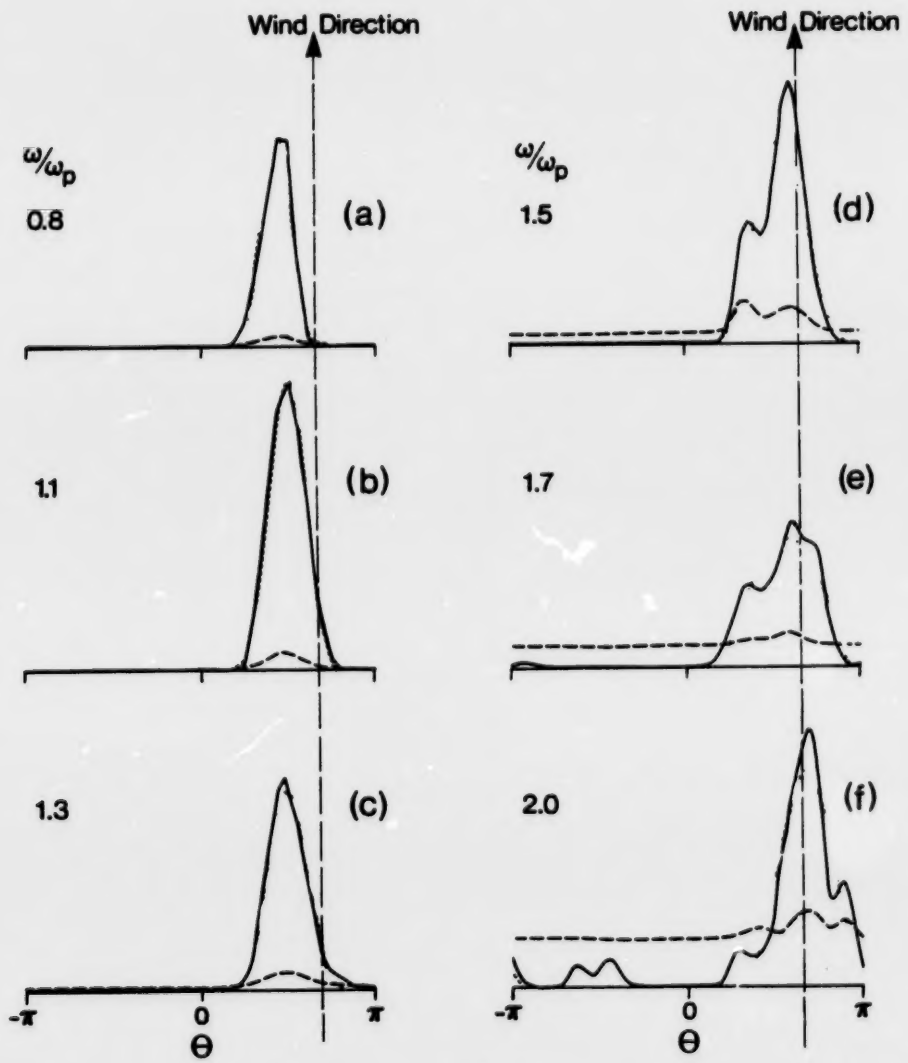

DIRECTIONAL SPECTRA $F(\omega,\theta)$

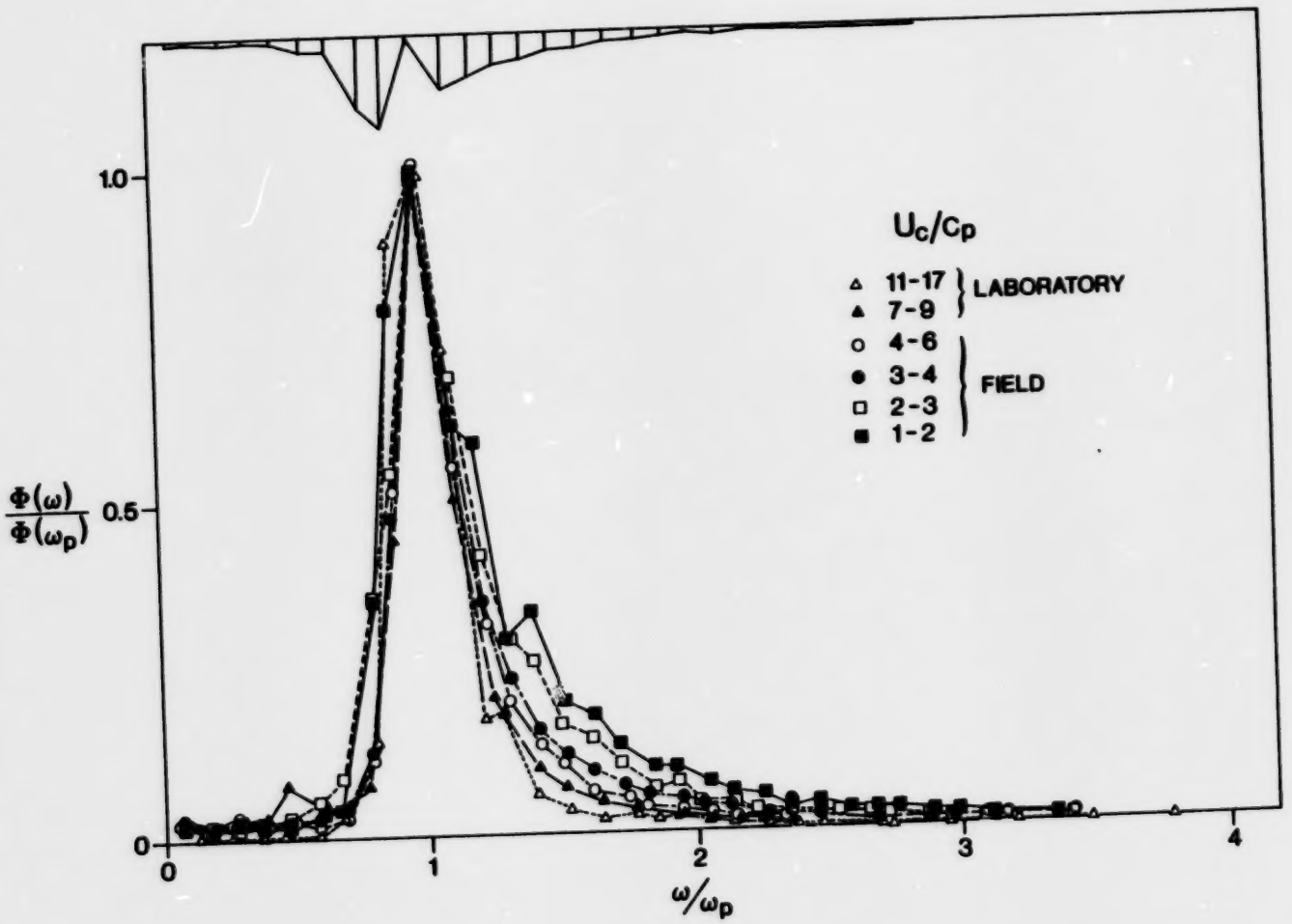
U_c/C_p
11-17
7-9
LABORATORY
4-6
3-4
2-3
1-2
FIELD
$\frac{\Phi(\omega)}{\Phi(\omega_p)}$
1.0
0.5
0
0
1
2
3
4
ω/ω_p

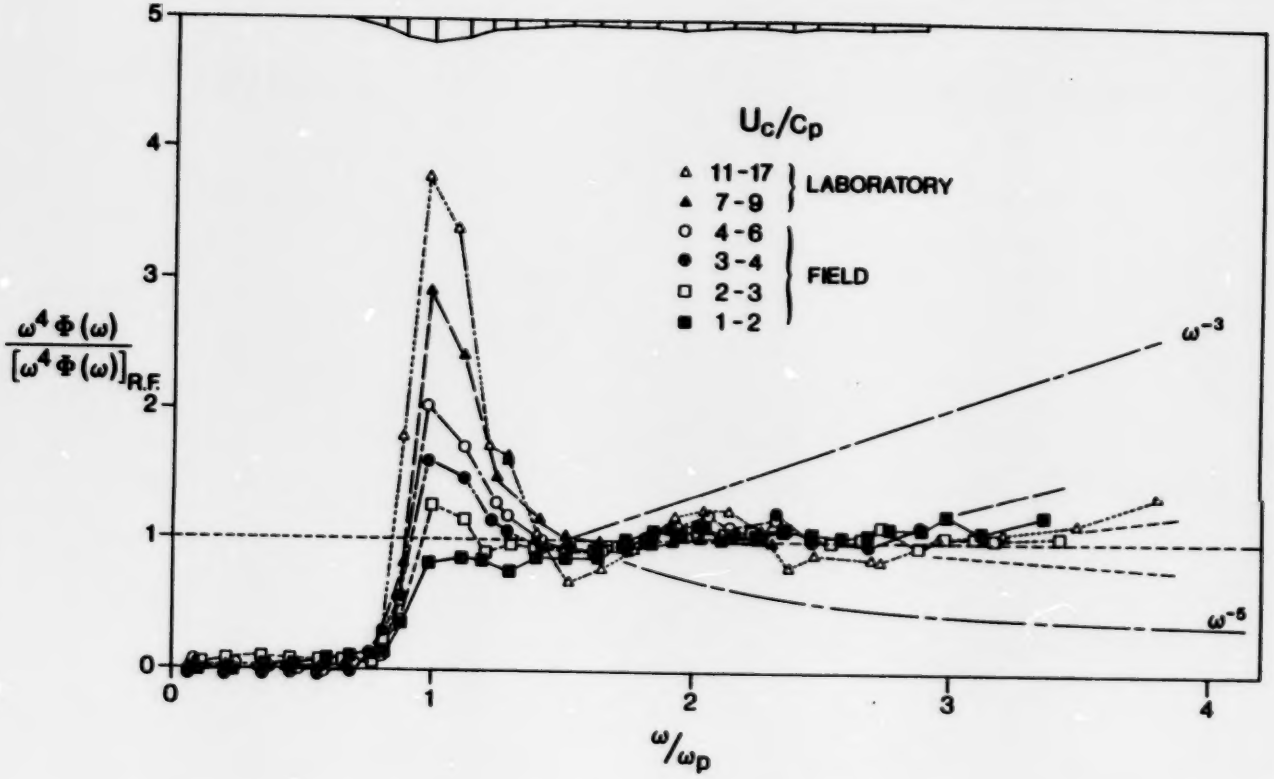
U_c/c_p
11-17
7-9
LABORATORY
4-6
3-4
2-3
1-2
FIELD
ω^{-3}
ω^{-5}
$\frac{\omega^4 \Phi(\omega)}{[\omega^4 \Phi(\omega)]_{R.F.}}$
ω/ω_p
0
1
2
3
4
5

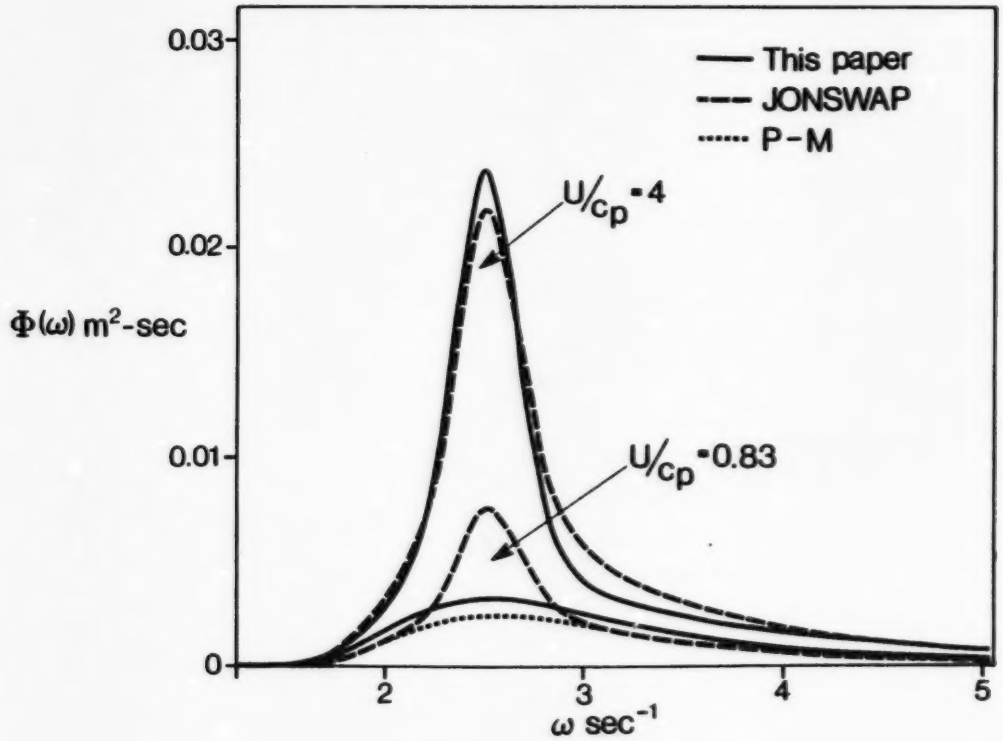
0.03
0.02
0.01
0
Φ(ω) m²-sec
This paper
JONSWAP
P-M
U/cp = 4
U/cp = 0.83
2
3
4
5
ω sec⁻¹

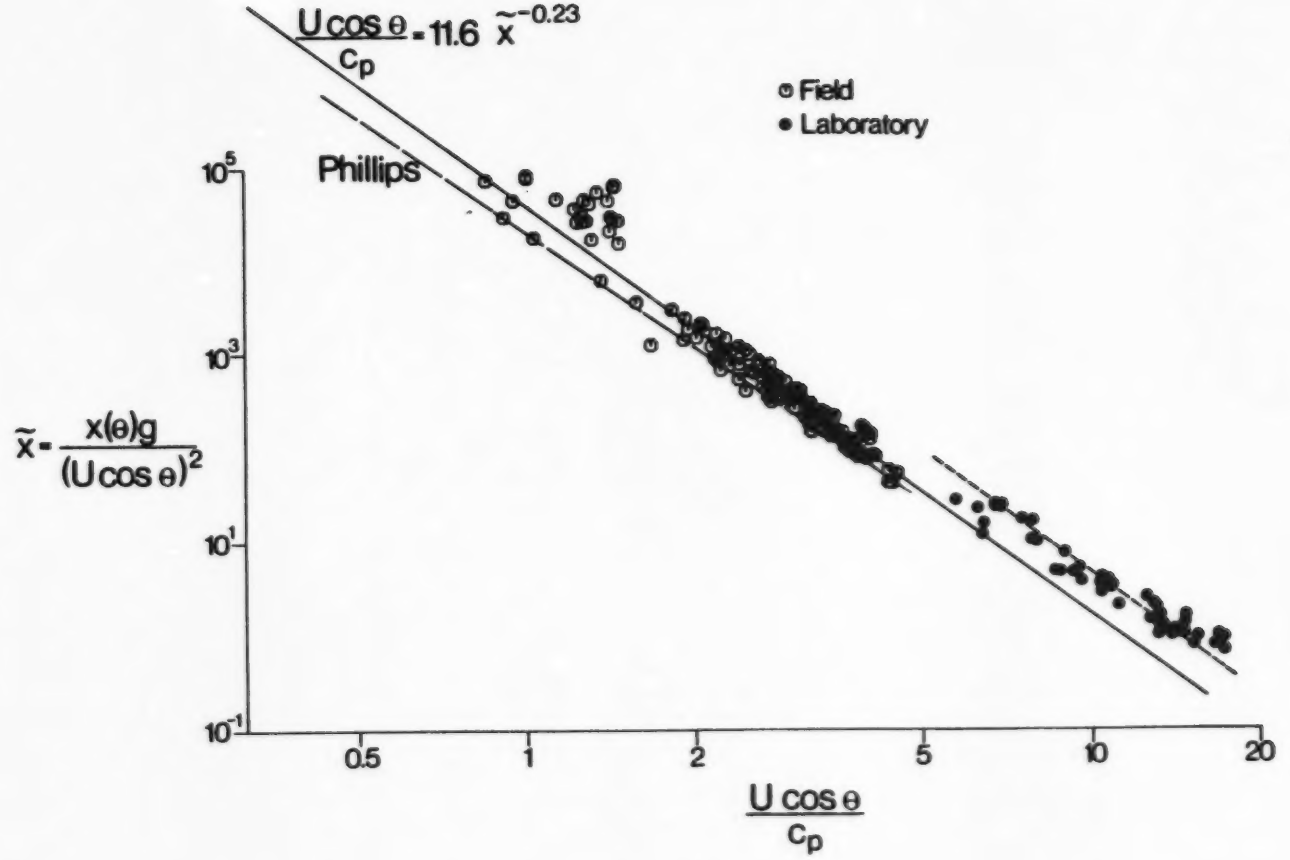
$\frac{U\cos\theta}{c_p} = 11.6\ \tilde{x}^{-0.23}$
Field
Laboratory
Phillips
10^5
10^3
10^1
10^{-1}
$\tilde{x} = \frac{x(\theta)g}{(U\cos\theta)^2}$
0.5
1
2
5
10
20
$\frac{U\cos\theta}{c_p}$

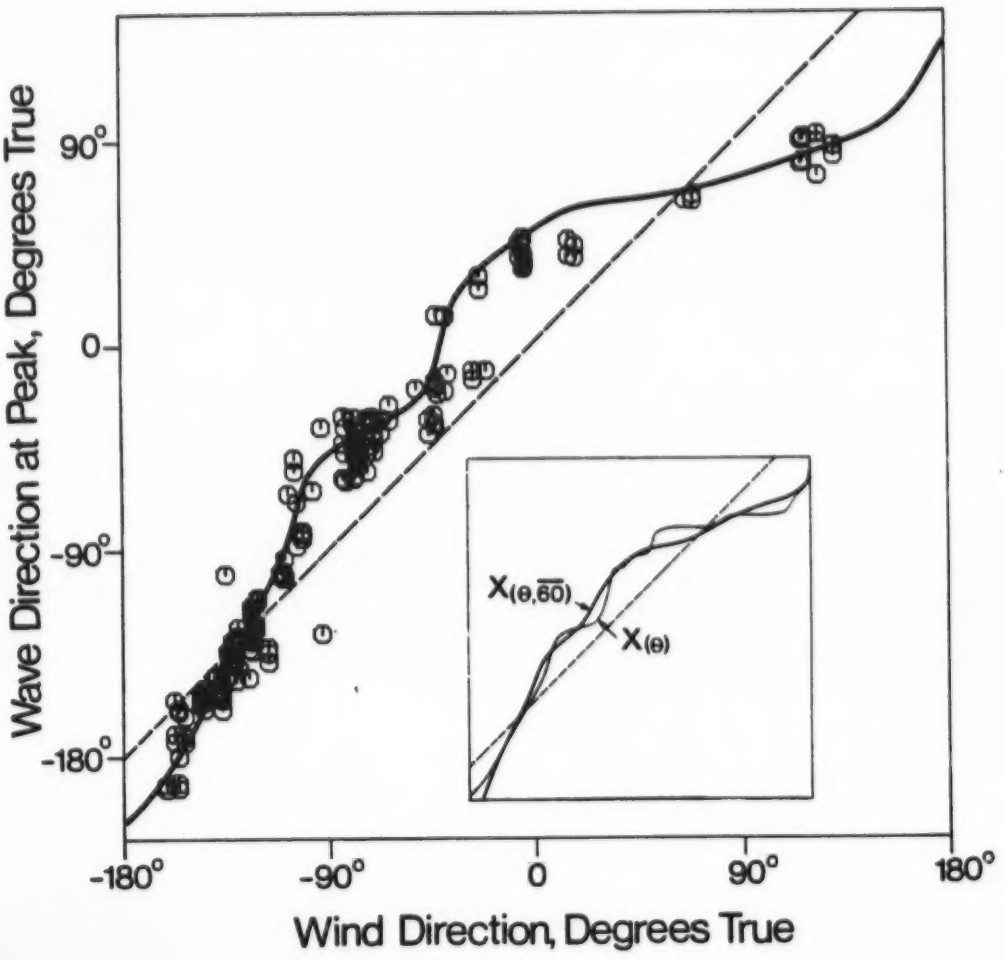
Wave Direction at Peak, Degrees True
90°
0
-90°
-180°
-180°
-90°
0
90°
180°
Wind Direction, Degrees True
$X_{(\theta,\overline{60})}$
$X_{(\theta)}$